Use of Electron Microscopy and Microdiffraction for Zeolite Framework Comparison

S. Nicolopoulos,[†,‡] J. M. González-Calbet,[*,†] M. Vallet-Regi,[‡] M. A. Camblor,[§] C. Corell,[§] A. Corma,[§] and M. J. Diaz-Cabañas[§]

Contribution from the Departamento de Química Inorgánica, Facultad de Químicas, and Departamento de Química Inorgánica y Bioinorgánica, Facultad de Farmacia, Universidad Complutense, 28040 Madrid, Spain, and Instituto de Tecnología Química, Universidad Politécnica de Valencia, UPV-CSIC, 47061 Valencia, Spain

Received October 23, 1996[⊗]

Abstract: Recent successful zeolite structure determination based on electron diffraction and image analysis data shows interesting prospects to characterize zeolitic frameworks provided the crystals are thin enough to produce useful crystallographic phases from image analysis. Zeolite SSZ-25 and porosil ITQ-1 structures were compared to reveal if they are isomorphous to MCM-22 zeolite. By using electron microdiffraction intensity data in the [0001] axis and phases extracted from HREM images taken at different defocus conditions, the resulting projected [0001] potential maps are found to be very similar for both structures and close to that of the MCM-22 zeolite.

Introduction

The properties of zeolites largely depend on their structures, which determine the size and shape of the intrazeolitic void volume (channels and cages). Thus, it is of importance to know the basic framework connectivity of zeolites, but it is usually difficult to apply direct single-crystal X-ray diffraction methods because of the usual microcrystalline nature of synthetic zeolites. As an alternative, we have very recently[1] described a method for direct structure determination from electron diffraction intensity data, and this was used to directly resolve the basal framework topology of zeolite MCM-22. Although electron diffraction techniques combining structure analysis by electron diffraction with HREM processing have largely been used[2−5] to solve a wide number of crystal structures (e.g., polymers, silicate minerals, proteins, etc.), this was the first example of structure determination in zeolites by such methods. The results agreed with an independent synchrotron X-ray diffraction powder and electron diffraction study[6] which indicated that the unit cell is hexagonal (*P*6/*mmm*) with $a = 1.48$ nm and $c = 2.68$ nm. In the same work, it was shown that the crystal structure of the three-dimensional framework contains two independent multidimensional channel systems with the largest rings of 10 and 12 tetrahedral atoms (10MR and 12MR). However, the minimum constricting apertures for both types of channels are 10MR, i.e., there are not 12MR channels, as zeolitic channels are defined by the size of the ring controlling diffusion through it.[7]

On the other hand, zeolite SSZ-25[8] and the pure silica material named ITQ-1[9] have been very recently synthesized and described, and the reported powder X-ray diffraction patterns suggest that these materials are isomorphous to zeolite MCM-22.[10] However, high-resolution electron microscopy of SSZ-25 was claimed to show the presence of at least one large pore in this zeolite,[11,12] in contrast with zeolite MCM-22 , which has no 12MR channels but 12MR supercages accesible through 10MR windows. If this were true, the conclusion would be that SSZ-25 and MCM-22 are not isomorphous. However, our ^{29}Si MAS NMR spectroscopy and adsorption measurements suggest that MCM-22, SSZ-25, and ITQ-1 are isomorphous.[9,13] The fundamental as well as the technical relevance of this problem has moved us to determine the basical aspects of the structures of SSZ-25 and ITQ-1 by direct electron crystallographic methods.

A recent work dealing with the possibility of direct electron crystallographic determination of zeolite structures shows that structure analysis based on diffraction data and crystallographic phases found by image analysis (Fourier filtration) gave interpretable potential maps in a 400 kV microscope[14] provided that crystal thickness is sufficiently small to minimize effects of dynamical diffraction.

In this paper, we describe how by making use of electron microdiffraction intensities and image analysis we can reconstruct the projected potential and, from this, we can compare the framework of the synthesized new materials SSZ-25 and ITQ-1. We also show that Moiré patterns formed when overlapping crystals are rotated by 30° around the *c*-axis enhance and directly resolve the basal framework. Thus, structural information supporting the isomorphism of SSZ-25, ITQ-1, and MCM-22 is obtained by means of electron microscopy.

[†] Facultad de Químicas, Universidad Complutense.
[‡] Facultad de Farmacia, Universidad Complutense.
[§] Universidad Politécnica de Valencia.
[⊗] Abstract published in *Advance ACS Abstracts,* October 15, 1997.

(1) Nicolopoulos, S.; González-Calbet, J. M.; Vallet-Regí, M.; Corma, A.; Corell, C.; Guil, J. M.; Perez Pariente, J. *J. Am. Chem. Soc.* **1995,** *117,* 8947−8956.
(2) Vainstein, B. K. *Structure Analysis by Electron Diffraction*; Pergamon Press: Oxford, U.K., 1964.
(3) Zvyagin, B. B. *Electron Diffraction Analysis of Clay Mineral Structure*; Plenum: New York, 1967.
(4) Dorset, D. L.; McCourt. M. P. *Electron Crystallogr. Trans.* **1992**, *28*, 105−113.
(5) Dorset, D. L. *Structural Electron Crystallography*; Plenum Press: New York, 1995.
(6) Leonowicz, M. E.; Lawton, J. A.; Lawton, S. L.; Rubin, M. K. *Science* **1994**, *264*, 1910−1913.
(7) Meier, W. M.; Olson, D. H. *Atlas of Zeolite Structure Types;* Butterworth-Heinemann: London, 1992.
(8) Zones, S. I. Eur. Pat. Appl. 231,860, 1987.
(9) Camblor, M. A.; Corell, C.; Corma, A.; Diaz-Cabañas, M. J.; Nicolopoulos, S.; González-Calbet, J. M.; Vallet-Regí, M. Submitted.
(10) Abril, R. P. L.; Bowes, E.; Green, G. J.; Marler, D. O.; Sihabi, D. S.; Sacha, R.F. U.S. Patent, 5,085,762, 1992.
(11) Pan, M.; Crozier, P. A. *Ultramicroscopy* **1993**, *52*, 487−458.
(12) Chan, I. Y.; P. A. Labun.; .Pan, M.; Zones, S. I. *Microporous Mater.* **1995**, *3*, 409−418
(13) Corma, A. Unpublished results.
(14) Dorset, D. L.; McCourt. M. P. *Microsc. Res. Tech. Trans.* **1997**, *26*, 212−223.

S0002-7863(96)03703-1 CCC: $14.00

Experimental Section

Materials. *N,N,N*-Trimethyl-1-adamantammonium Hydroxide (TMAdaOH): 1-Adamantamine (4.667 g) was dissolved in 50 g of chloroform. Then, 11.350 g of $K_2CO_3 \cdot 1.5H_2O$ was added and the mixture was cooled in an ice bath. Then, 13.14 g of CH_3I was added. The next day a second portion of CH_3I (6.5 g) was added. After 5 days, the mixture was filtered and the solid washed with $CHCl_3$. The $CHCl_3$ solution was rotovaporated under vacuum. A 96.3% yield (on amine basis) of $C_{13}H_{24}N^+I^-$ was obtained (chemical analysis: 4.54% N, 48.62% C, 7.56% H; theoretical: 4.36% N, 48.61% C, 7.53% H). The iodide was converted to the hydroxide by anion exhange with Dowex 1 resin.

Zeolite SSZ-25:[8] KOH (0.585 g) was dissolved in 27.018 g of a 0.65 M solution of 1-TMAdaOH. Then 0.268 g of alumina (Pural SB Condea, 74.6% Al_2O_3, 25.4% H_2O) and 35.935 g of water were added, and the mixture was stirred for 4 h. Then, 12.66 g of colloidal silica (Ludox AS-40,40%SiO_2) was added and the mixture stirred for 2 h. The resultant reaction mixture was then transferred to PTFE line stainless steel 60 mL autoclaves which were heated in an oven at 448 K while being tumbled at 60 rpm. After 7 days of heating the autoclaves were quenched and the contents filtered, washed with water until pH < 9, and dried at 373 K. A portion of the solid was calcined at 853 K in air. The product has a Si/Al molar ratio of 27.4.

Pure Silica ITQ-1: A 0.525 M solution of 1-TMAdaOH (10.442 g) was mixed in the PTFE liner of an autoclave with 5969 g of water, then 1.22 g of amorphous silica (Aerosil 200, Degussa) was added and the mixture was stirred for 2 h. Then, the gel was heated in an autoclave at 423 K for 14 days while being tumbled at 60 rpm. Afterward, the autoclave was quenched and the contents were filtered and washed with water until pH < 9 and dried at 373 K. The product was calcined in air at 853 K.

Zeolite MCM-22:[15] NaOH (0.454 g) and 5.76 g of hexamethyleneimine were disolved in 94.16 g of deionized water. Then, 0.212 g of sodium aluminate (Carlo Erba, 56% Al_2O_3 37% Na_2O) was added and the mixture stirred until a clear solution was obtained. Then, 6.99 g of colloidal silica (Aerosil 200, Degussa) was added and the mixture stirred for 30 min. The mixture was transferred to PTFE line stainless steel autoclaves and heated in an oven at 408 K for 11 days while being tumbled at 60 rpm. The autoclaves were then quenched and the contents filtered and washed with water until pH < 9. The solid was dried at 373 K and then calcined at 853 K. The molar Si/Al ratio of the product was 50.

Image Processing and Instrumentation. Powder XRD data were collected on a Philips 1060 diffractometer equipped with graphite monochromator and using Ni-filtered Cu Kα radiation ($\lambda = 0.1542$ nm). Transmission electron microscopy (TEM) observations were performed on a JEOL 4000EX operated at 400 kV ($C_s = 1$ mm, $C_c = 1.7$ mm) and equiped with a top-entry double-tilt specimen holder. Specimens for HREM observations were obtained by dry dispersion on copper grids covered with holey carbon film. HREM micrographs were scanned with an EPSON GT900 and processed with the CRISP software[16] run on a Pentium 120 MHz/Intel computer. Digitization and calculation of Fourier transforms (FT) of the images was done as described elsewhere.[17] The FT of the image sampled at reflection spot centers was used to derive crystallographic phases and amplitudes. Processing algorithms are all based on the system developed at the MRC Laboratory of Molecular Biology in Cambridge.[18] Intensities of reflections were extracted from the microdiffraction patterns by integrating intensities (as gray levels) on reflection disks.

When an image is taken near Scherzer-focus conditions (−48 nm at 400 kV), all reflections within the resolution limit of the microscope are recorded with the correct phase. Images that are not recorded at exactly the Scherzer-focus conditions show a number of dark rings (contrast transfer function (CTF) crossovers) on the calculated FT. When such crossovers are found, the CTF changes sign and the reflections change phase by exactly 180° (i.e., they are reversed in contrast, making black white and vice-versa).

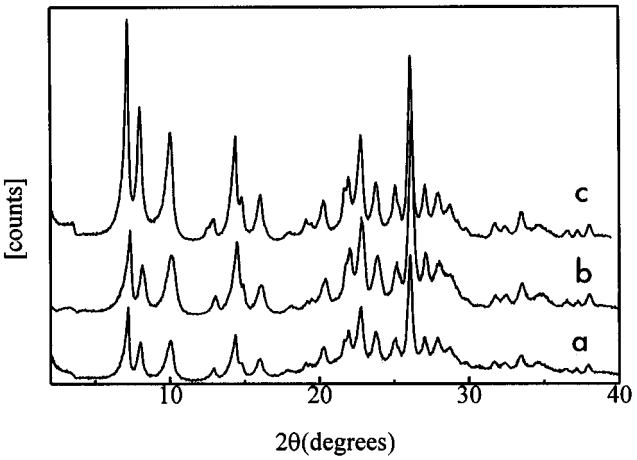

Figure 1. Powder XRD patterns of calcined (a) SSZ-25, (b) ITQ-1, and (c) MCM-22.

Thus, according to the theory,[19] an image which is taken at such defocus conditions, it has a complex mixture of Fourier components; some have the correct contrast and some reversed. The "CTF correction" we applied in our HREM images (integrated as a filter in the CRISP package) consisted of the CTF compensation, i.e., by adding 180° to the phases of the reflections lying in ranges where the CTF changes sign (i.e., reflections are reversed in contrast).

Results

Powder XRD data (Figure 1a,b) and electron diffraction studies suggest a hexagonal unit cell with parameters $a = b =$ 1.43 nm and $c = 2.65$ nm before and after calcination (e.g., very close to the MCM-22 structure, see for comparison Figure 1c). Before calcination, MCM-22, SSZ-25, and ITQ-1 contain also a layered material which is thought to be a precursor of the zeolite, this being formed by condensation of T−OH or TO− groups thoughout the layers.

To proceed to the direct crystallographic determination of the unknown zeolite framework structures, we need electron diffraction intensity data and corresponding phases extracted by image analysis (Fourier filtration) from the same projections. The symmetries of unknown structures can be determined by different methods; electron microdiffraction patterns provide reliable information for differentiating without ambiguity between different symmetries.[20]

The [0001] microdiffraction (MDF) patterns for all examined samples were found to be exactly similar (Figure 2a−c) presenting a (6*mm*) "ideal" symmetry in the zero-order Laue zone (ZOLZ) coresponding to the *p*6*mm* plane group. Intensities of equivalent reflections measured on the same pattern were compared, and the crystallographic R_{sym} value was always less than 10%. The (6*mm*) symmetry is exactly reproducible over several examined crystals in the (*hki*0) plane for both structures and exactly similar to the symmetry of the (hki0) pattern of the MCM-22 structure (Figure 2d).

Although all the examined samples were extremely beam-sensitive and became amorphous within seconds, we could obtain HREM images along [0001] (Figure 3a−c). Those HREM images were taken from a thin part of the crystal and were subsequently digitized and processed; symmetry determination of unknown structures can also be determined by experimentally observed phases in HREM images. These phases can be used for symmetry determination, since phase relations and restrictions are different for different symmetries.

(15) Corma, A.; Corell, C.; Perez-Pariente, J. *Zeolites* **1995**, *15*, 2−8.
(16) Hovmoller, S. *Ultramicroscopy* **1992**, *41*, 121−135.
(17) Hovmoller, S.; Sjogren, A.; Farrants, G.; Sundberg, M.; Marinder, B. O. *Nature* **1984**, *311*, 238−241.
(18) Amos, L. A.; Henderson, R.; Unwin, P. N. T. *Prog. Biophys. Mol. Biol*. **1982**, *39*, 183−231.
(19) *International Tables for Crystallography*; Kluwer Academic Publishers: London, 1993; Vol. B, pp 280−329.
(20) Mornirolli, J. P.; Steeds, J. W. *Ultramicroscopy* **1992**, *45*, 219−239.

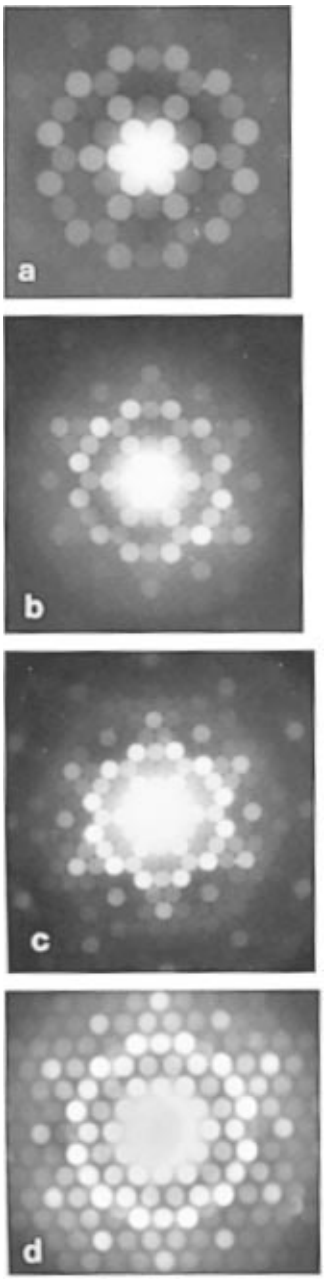

Figure 2. Microdiffraction patterns corresponding to SSZ-25 structure along [0001] (a) before and (b) after calcination and the same patterns for calcined (c) ITQ-1 and (d) MCM-22. All patterns are similar and exhibit (6*mm*) "ideal" symmetry.

The data quality is quantified using a figure of merit R_A and R_ϕ:

$$R_A = \frac{\sum(|A_{obs}(hk)| - |A_{S_{sym}}(hk)|)}{\sum|A_{sym}(hk)|}$$

where A_{obs} is the observed amplitude and A_{sym} is the amplitude which fulfils the characteristics of the particular plane symmetry and

$$R_\phi = \frac{\sum(w(hk)|\phi_{obs}(hk)| - |\phi_{sym}(hk)|)}{\sum w(hk)}$$

where R_ϕ is the averaged phase error (phase residual) of symmetry related reflections, $w(hk)$ is a weighting factor given to a reflection (hk), usually set to be equal to the amplitude of the reflection (hk); $\phi_{obs}(hk)$ is the experimentally observed phase and $\phi_{sym}(hk)$ is the phase which fulfils the characteristics of the particular plane symmetry. Since different symmetries have different relations and restriction for phases, phase residuals for an image will be different for different symmetries. Once the phase residuals R_ϕ for individual symmetries are calculated, the symmetry of the crystal can be deduced by comparing those phase residuals (see Table 1). As we can observe from this table, amplitude residuals R_A are similar for all the considered

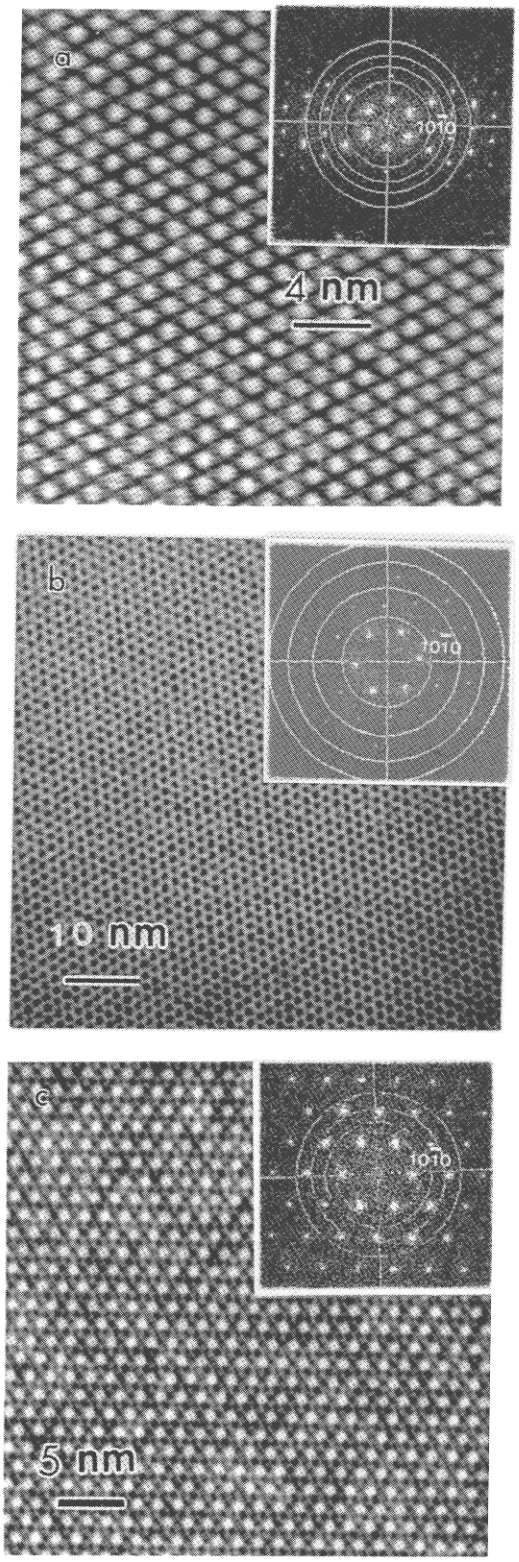

Figure 3. HREM micrographs along [0001] orientation of SSZ-25 (a) before and (b) after calcination and of (c) calcined ITQ-1. In the corresponding insets are shown the FTs of the scanned images. A set of circles (available as a filter tool in CRISP software) are fitted to the dark rings corresponding to the zero crossovers of the CTF.

Table 1. Calculated Amplitudes and Phase Residuals for Different Crystal Symmetries for As-Made SSZ-25 (I), Calcined SSZ-25 (II), and Calcined ITQ-1(III) Zeolites

plane symmetry	R_A (%)			Φ_{res}		
	I	II	III	I	II	III
*p*3	32.3	10.4	20.1	2.8	4.2	7.2
*p*3*m*1	32.3	10.4	20.1	6.1	4.6	8.6
*p*31*m*	32.3	10.4	20.1	5.8	8.6	7.2
*p*6	32.3	10.4	20.1	7.1	8.7	8.6
*p*6*mm*	32.3	10.4	20.1	7.0	8.8	8.5

plane groups and the R_ϕ residuals for the p3 plane group are the lowest; however, all remaining plane groups have very similar R_ϕ. In such case, it is not unreasonable to consider the correct group to be the one of the highest symmetry, i.e., *p*6*mm*.[21] Such conclusion can be further supported by the observed symmetry of the [0001] (MDF) patterns corresponding to the *p*6*mm* plane group.

From the inset optical diffraction patterns (Figure 3a−c), we can see that in both images reflections extend up to 0.24 nm resolution; the position of the observed CTF crossovers indicates that those HREM images were taken away from the Scherzer defocus. However, according to the theory,[18] only under weak phase approximation (Sherzer defocus and thin part of the crystal) do HREM images directly show interpretable projected framework potential.

By interactively drawing the positions and the sizes of the rings showing zeros of the CTF (in the FT of the images), we can determine it and estimate the defocus conditions under which the micrograph was taken; those micrographs were estimated to be taken at a focuses of 450, 850, and 940 nm (Figure 3a−c, respectively).

Calculated phases are relative to a phase origin; in centrosymmetric projections, the phases should be exactly 0° or 180° if the origin is at a center of symmetry. The unit cell origin is usually chosen at a point of high symmetry, in accordance with conventions defined in ref 22. Only with this origin will the structure factors phases obey the symmetry rules for the structure. The origin refinment is based on the principles implemented in the MRC programs;[18] phase origin determination is done by searching through the unit cell for the position with the best agreement between observed phases of symmetrically equivalent structure factors and the known symmetry constraints.

As long as the (6*mm*) "ideal" symmetry of the [0001] axis corresponds to a *p*6*mm* projection plane symmetry which is centrosymmetric, all (*hki*0) phases are set to either 0° or 180°. For the plane group *p*6*mm*, the following relations restrictions hold between symmetry-related amplitudes and phases (T_1):

$$F(hk) = F(k\bar{h}\bar{k}) = F(\bar{h}\bar{k}h) = F(kh) \quad \text{for structure factors}$$

$$\phi(hk) = \phi(k\bar{h}\bar{k}) = \phi(\bar{h}\bar{k}h) = \phi(kh) \quad \text{for phases}$$

These symmetry constraints were imposed on amplitudes and phases obtained from HREM and image analysis. Again, as we commented before, the "CTF correction" (integrated as a filter in the CRISP package) we applied in the HREM micrographs consisted of the CTF compensation, i.e., by adding 180° to the phases of the reflections lying in ranges where the CTF has negative values.

Table 2. Normalized E_{hki0} Amplitudes for As-Made SSZ-25 (I), Calcined SSZ-25 (II), and Calcined ITQ-1 (III) Zeolites

*hki*0	I	II	III
1010	1.45	1.2	1.12
2020	0.95	0.78	0.73
3030	1.01	0.78	0.81
1120	0.82	0.75	0.71
2240	1.12	0.82	0.92
3140	1.85	1.37	1.38
3250	0.48	1.22	1.29
5050	0.59	0.92	0.91
3360	0.81	0.94	1.02
2130	1.10	0.94	1.02

While calculated amplitudes from the FT of Figure 3 could be affected by crystal tilt and attenuated by the CTF of the microscope, we used electron diffraction intensities from the individual electron MDF patterns of Figure 2a−c to reconstruct the [0001] potential map. Electron microdiffraction patterns are not affected by the CTF and provide symmetry information from very small areas of the crystal.

In Table 2 we observe the normalized electron diffraction amplitudes corresponding to MDF patterns of Figure 2a−c; normalized structure factors are calculated from the observed ED structure factor magnitudes $|F_{hki0}|_{obs}$, i.e.

$$|E_{hki0}|^2 = |F_{hki0}|^2/\epsilon\sum f_i^2$$

where F_{hki0} stands for observed structure factor magnitudes, f_i for electron scattering factor values,[25] and ϵ a term to correct zones with systematic absences. The normalization of the $|E_{hki0}|$ set is achieved by requiring $\langle|E|^2\rangle = 1.000$.

The (*hki*0) projection potential map was then reconstructed by inverse Fourier tansformation (Figures 4a−c, 5a−c, and 6a−c) for all the samples using phases (corrected for the CTF) and normalized amplitudes. As we can observe, they are similar for the as-made and calcined SSZ-25 and calcined ITQ-1. Moreover, they are similar to the (*hki*0) potential map of the MCM-22 structure (Figure 8a in ref 1), revealing the same projection basal framework for all structures (Figure 7). It is also very important to note that CTF correction but especially the use of normalized intensities greatly improves the resolution of the final potential maps (Figures 4c, 5c, and 6c).

On the other hand, HREM images show that all of the studied zeolite structures are faulted at a nanometric level, with boundaries separating different overlapping crystallites forming Moiré interference patterns. In the case of the MCM-22 structure, projection of the framework topology can be remarkably enhanced by the Moiré effect.[1] In fact, in the special case in which overlapping crystallites along the (0001) direction are rotated by 30° with respect to one another around the *c*-axis, rotational hexagonal Moiré patterns are formed which enhance and directly resolve the projected zeolite framework topology (Figure 8a,b). In these figures, details within the Moiré patterns seem to be related by the *p*6*mm* symmetry; as can be observed by carefully inspecting the white dot pattern within the Moiré supercell (Figure 8a), large symmetrical white rings appear to be bounded by smaller pentagonal rings, showing that way a striking similarity with the projected basal framework connectivity of the MCM-22 structure (Figure 7).[6] Similar Moiré patterns (i.e., showing similar 12-fold arrangement of bright dots) have also been observed in all studied zeolites, indicating the same (basal) framework for all structures.

Again, to reveal the 3D framework topology, we need at least one [1120] and/or [1010] potential map projection. Unfortu-

(21) Valpuesta, J. M.; Carascosa, J. L.; Henderson, R. *J. Mol. Biol.* **1994**, *240*, 281−287.
(22) *International Tables for Crystallography*, Kluwer Academic Publishers: London, 1989; Vol. A.
(23) Doyle, P. A.; Turner, P. S. *Acta Crystallogr.* **1968**, *A24*, 390−397.
(24) Ramachadran, G. N.; Srinvasan, R. *Fourier Methods in Crystallography*; Wiley Interscience: New York, 1970; pp 62−67.
(25) Dorset, D. L.; Kopp, S.; Fryer, J. R.; Tivol, W. F. *Ultramicroscopy* **1995**, *57*, 59−68.

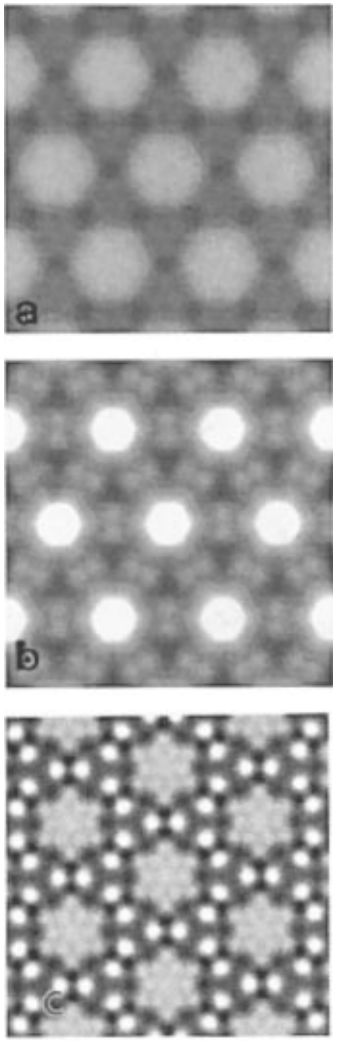

Figure 4. [0001] projection potential maps (3 × 3 cells) for as-made SSZ-25 calculated (a) after imposing *p*6*mm* crystallographic symmetry and before CTF correction, (b) after CTF correction, and (c) after CTF correction and imposition of normalized amplitudes.

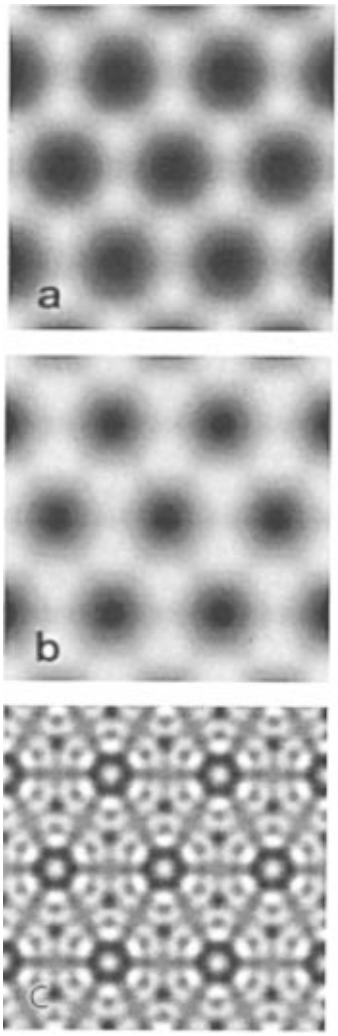

Figure 5. [0001] projection potential maps (3 × 3 cells) for calcined SSZ-25 calculated (a) after imposing *p*6*mm* crystallographic symmetry and before CTF correction, (b) after CTF correction, and (c) after CTF correction and imposition of normalized amplitudes.

nately, corresponding MDF patterns for SSZ-25 and ITQ-1 structures when obtained are of bad quality for precise ED intensity measurements as they are affected by local tilts, crystal bending, or quick radiation damage. Furthermore, although crystallographic phases can still be extracted from such images, there is a serious risk that such phases are wrong due to excessive crystal thickness along the corresponding [1120] and/or [1010] direction.

Discussion

First, it is very interesting to note that as long as the (*hki*0) MDF patterns of SSZ-25 and ITQ-1 are strikingly similar and also similar to the MCM-22 symmetry MDF pattern, a direct structure determination based on a probabilistic estimate of phases of different ED intensities as presented in ref 1 would lead to similar projection basal framework topology for the three studied zeolites.

Alternatively, in this work, we describe how by using diffraction intensities and crystallographic phases found by image analysis—provided the crystal is thin enough—we can reconstruct the correct projected potential and subsequently reconstruct the correct zeolites framework.

Recent results of structure analysis on zeolites[14] based on simulated electron micrographs and diffraction intensities which are perturbed by multiple scattering reveal that ab-initio phasing techniques could be applied for determining the structures of zeolites at atomic resolution; in fact, provided that the crystal thickness is less than 15 nm and the experimental voltage is sufficiently high, observed data, i.e., electron diffraction intensities (although contaminated by dynamical and secondary scattering) and phases extracted from image analysis are still useful for structure analysis. According to our micrographs, the examined samples have platelet forms of thickness around 12 nm.

As we have mentioned before, only HREM images of thin crystals taken at Scherzer defocus represent directly the projected framework potential; otherwise the structural information which is still present in the images is distorted. Such distortions can be compensated for by image analysis, so correct values for both amplitudes and phases of structure factors can be retrieved and the potential maps revealing the correct crystal framework can be reconstructed.

Generally speaking, in a structure determination, the phases are more important for solving the structure,[24] while amplitudes are important for refining the structure. As long as the phases are correct, errors in the amplitudes do not completely change the atomic positions, but mainly make the relative peak heights less accurate. However, depending on the electron wavelength used, there seems to be a limit in thickness where beyond that phases extracted from images are wrong for crystal determination.[14]

We can observe that, using uniquely amplitudes extracted from (*hki*0) HREM images, the resulting (*hki*0) potential maps

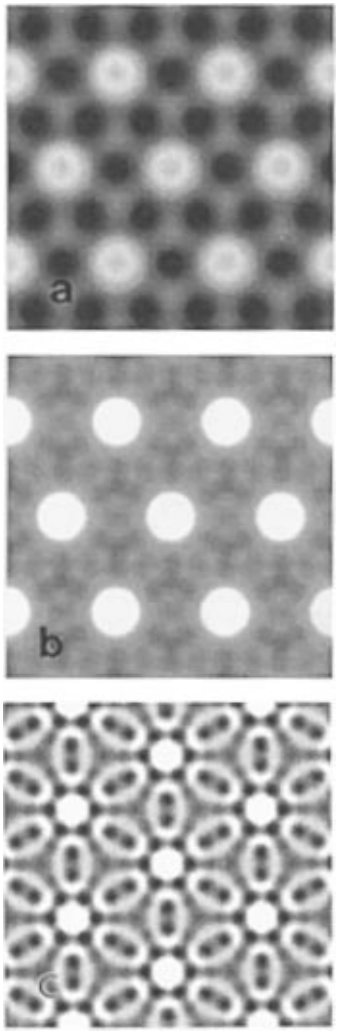

Figure 6. [0001] projection potential maps (3 × 3 cells) for calcined ITQ-1 calculated (a) after imposing *p*6*mm* crystallographic symmetry and before CTF correction, (b) after CTF correction, and (c) after CTF correction and imposition of normalized amplitudes.

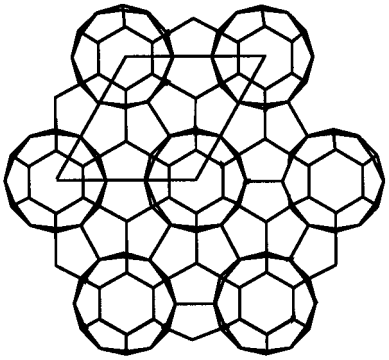

Figure 7. Projected basal framework model for the MCM-22 structure. Only T atoms are considered.

are of poorer resolution (Figures 4b, 5b, and 6b); this means that the moduli of structure factors obtained from the electron diffraction intensity as a whole are more reliable than those obtained from the image, even when the EDP is not taken from the same sample area as the image. One of the reasons might be due to the oscillation of CTF. Errors might occur for those

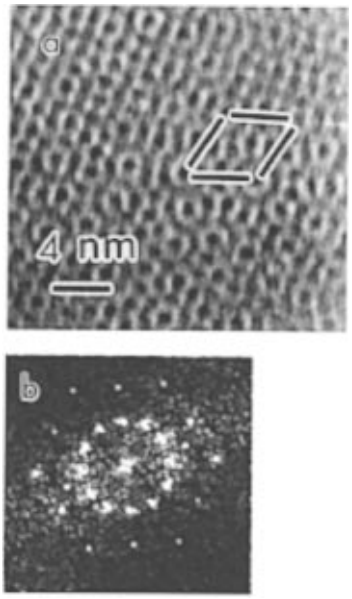

Figure 8. (a) HREM image along [0001] showing superimposed crystals of porosil ITQ-1 with relative rotation of 30°. White "rings" of 12-fold symmetry are clearly seen within the observed Moiré pattern. (b) Corresponding diffractogram having a 12-fold symmetry.

structure factors which have a diffraction vector corresponding to a zero or very small value of CTF, when the structure factors are obtained from the Fourier transform of the image.

Therefore, the use of ED intensities of the observed MDF patterns seems more reliable and precise. The use of normalized structure factors enhances the structural details of the [0001] potential map and has also been succesfully used elsewhere for structure image resolution enhancement and determination.[26,27]

Conclusion

In the present paper, we use electron crystallography techniques to reveal whether unknown zeolite structures are isostructural (or not) with the MCM-22 structure. Up to now, HREM images have often been used for rough interpretation of zeolite frameworks. Such framework resolutions are generally inaccurate as often HREM images are away from the ideal conditions (Scherzer defocus) and image artifacts may be present.[27] Therefore, such structure models deduced from the HREM images must be verified by comparison with computer-simulated images. One of the disadvantages of image simulation is that enormous amounts of images need to be calculated if all the optical parameters have to be scanned in small steps.

Zeolite framework resolution (and comparison) can be done alternatively by using electron diffraction data and image analysis as long as HREM images contain useful both amplitude and phase information.

The conclusion of our study is that SSZ-25 and porosil ITQ-1 seem to have a similar, large 12MR pore along the c-direction: the projected framework topologies of those structures seem to be equivalent to that of the MCM-22 zeolite. Whether those structures are completely isomorphous to the MCM-22 structure or not is a question that can be adressed using also image analysis of other (i.e., [1010] or [1120]) projections, provided that sufficiently thin sections corresponding to those orientations can be prepared to collect reliable crystallographic phases.

JA963703I

(26) Hu, J. J.; Li, F. H.; Fan, H. F. *Ultramicroscopy* **1992**, *41*, 387−397.

(27) Terasaki, O. *J. Electron Microsc.* **1994**, *43*, 337−346.